J Grid Computing (2022) 20: 23
https://doi.org/10.1007/s10723-022-09615-0

A Deep Learning and Handcrafted Based Computationally Intelligent Technique for Effective COVID-19 Detection from X-ray/CT-scan Imaging

Mohammed Habib · Muhammad Ramzan · Sajid Ali Khan

Received: 28 October 2021 / Accepted: 27 June 2022 / Published online: 18 July 2022

Abstract The world has witnessed dramatic changes because of the advent of COVID19 in the last few days of 2019. During the last more than two years, COVID-19 has badly affected the world in diverse ways. It has not only affected human health and mortality rate but also the economic condition on a global scale. There is an urgent need today to cope with this pandemic and its diverse effects. Medical imaging has revolutionized the treatment of various diseases during the last four decades. Automated detection and classification systems have proven to be of great assistance to the doctors and scientific community for the treatment of various diseases. In this paper, a novel framework for an efficient COVID-19 classification system is proposed which uses the hybrid feature extraction approach. After preprocessing image data, two types of features i.e., deep learning and handcrafted, are extracted. For Deep learning features, two pre-trained models namely ResNet101 and DenseNet201 are used. Handcrafted features are extracted using Weber Local Descriptor (WLD). The Excitation component of WLD is utilized and features are reduced using DCT. Features are extracted from both models, handcrafted features are fused, and significant features are selected using entropy. Experiments have proven the effectiveness of the proposed model. A comprehensive set of experiments have been performed and results are compared with the existing well-known methods. The proposed technique has performed better in terms of accuracy and time.

Keywords COVID-19 detection · Medical images · Handcrafted features · Deep learning · Weber local descriptor · X-ray · CT scan

1 Introduction

Different methods of COVID-19 detection have been in practice during the last two years. In one of the most common approaches, respiratory samples collected from suspected COVID-19 patients are used for the detection of the presence of antigens. According to the recommendations of the World Health Organization (WHO) Real-Time Polymerase Chain Reaction (RT-PCR) test is being used for the diagnosis of COVID-19 patients [1]. Different research has been carried out to measure the presence of disease amongst the target population. In one such paper, results taken from the sample of 64 patients using RT_PCR were reported to

M. Habib · M. Ramzan
Department of Computer Science, College of Computing and Informatics, Saudi Electronic University, 11673 Riyadh, Saudi Arabia

M. Habib (✉)
Department of Electrical Engineering, Faculty of Engineering, PortSaid University, Port Said 42526, Egypt
e-mail: mhabib@seu.edu.sa

S. A. Khan
Department of Software Engineering, Foundation University Islamabad, 44000 Islamabad, Pakistan

have a sensitivity of 91% approximately [2]. One of the major concerns is that diagnosis time using this methodology takes more time approximately a few hours to two days. In other approaches, different techniques are used. For example, respiratory samples can also be used for the detection of viral proteins in the COVID-19 samples using Rapid Diagnostic Test (RDT). It is a faster way of detection in a few minutes but relatively low sensitivity has been reported in confidence intervals from 34 to 80% [3]. Another major concern is that these results are highly dependent on the quality and quantity of antigens. Onset time is also an important factor for covid-19 diagnosis. In COVID-19 patients antibodies takes approximately two weeks to develop which causes hindrance in early detection. Deep learning (DL) and the Internet of Things (IoT) also play important role in healthcare applications [4, 5]. Multiple hidden layers are deployed in DL methods for solving complex pattern recognition problems. DL is widely used in healthcare applications such as ulcer detection [6, 7], predicting the risk of heart failure [8], discovering the gait patterns which reveal the neurodegenerative diseases [9], Abnormal Behavior Detection [10], Dim Target Detection [11], Emotion Recognition [12] and classifying ECG signal database [13].

There are multiple image modalities such as CT-Scan images, X-Ray images, and Ultrasound images, which are not only used for the detection and diagnosis of COVID-19 but also for estimating synthetic CT [14], Brain Tumor Segmentation [15] and medical image security [16]. Patients with symptoms at earlier stages have been found to have ground-glass opacities. Patients in later stages demonstrate blockage in the pulmonary arteries as another pattern. These two categories have been found consistent and are helpful in the detection process [17, 18]. In the past as well, Pneumonia has been detected using chest images and has been effectively analyzed using machine learning techniques. This offers a unique challenge to deploy Machine Learning techniques for the detection of COVID symptoms. That is because COVID symptoms have many similarities with infections caused by pneumonia. The problem becomes even more challenging and involves human intervention. It results in a longer duration for detection and ultimately causes a delay in curing the patients. Automated detection with improved accuracy has become a significant challenge and requires more attention.

2 Related Work

Considering the scope of the problem and the significance of COVID-19 detection and diagnosis, researchers are working on its solutions especially in the domain of computer vision and deep learning [19, 20]. These solutions are not only cheaper but also reliable. Automated diagnosis can greatly help medical experts inefficient decision-making. Even it can greatly help the developing countries where there is a shortage of field experts. Recently many solutions have been proposed using CT-Scan, X-ray images, and ultrasound images. However, there is still room for a better and automated fast detection mechanism [21].

As discussed earlier the symptoms of COVID-19 are like pneumonia, therefore, it is required to uniquely identify the COVID-19 patterns against the patterns observed in the form of pneumonia. Numerous studies on COVID-19 have been reported in the literature. The accuracy of COVID-19 detection mainly depends on the type of features extracted from images. The feature extraction methods of COVID-19 fall into these categories: Traditional handcrafted (HC) features [22–25] and deep learning methods [26–29]. Here we present the state of research related to these methods.

2.1 Traditional Handcrafted (HC) Feature Methods

HC feature methods are used for decades and are still powerful tools when combined with machined learning classifiers. Maheshwari et al. [22] propose a Local binary pattern-based intelligent system for COVID-19 detection. The features are extracted from Local binary pattern (LBP) images and chest x-ray images and jointly investigated. Thus, highly discriminatory features are obtained and provided to the classifier to achieve the 97.97% accuracy rate. Tuncer et al. [23] used both exemplar LBP and LBP together to extract high-level, middle-level, and low-level features. A new iterative RelieF based feature selection method is also presented in this work for a selection of relevant features. Subspace discriminant (SD), k nearest neighborhood (kNN), support vector machine (SVM), linear discriminant (LD), and Decision tree (DT) classifiers are used in the classification step. They reported a classification accuracy rate of 100% using SVM. Mostafiz et al. [24] combined the features of

discrete wavelet transform (DWT) along with deep CNN for COVID-19 detection. Recursive feature elimination (RFE) along with maximum relevance and minimum redundancy is used for optimal feature selection. A random forest-based bagging method is used for testing the proposed method and an accuracy rate of 98.5% is achieved. Pustokhina et al. [25] also combined DWT features with a rough neural network (RNN) to develop a machine learning-based model named DWT-RNN. Before the classification step, the subset of features is reduced using principal component analysis (PCA). Similarly, in another study [30] the authors detect COVID-19 using a wavelet-based convolution neural network. They considered different wavelet families like discrete Meyer, Coiflt, Biorthogonal, Symlet, Daubechies, and Haar to execute DWT. The two-level decomposition of DWT is performed to suppress the noise effect and extract the prominent features from X-ray images. On average 98% accuracy rate was obtained during the testing phase. Imani [31] explored the limitation of deep learning methods and proposes an efficient convolution filter named CFRCF. The textural and shape features are extracted from CT and X-ray images using CFRCF. Moreover, contextual features are extracted using Attribute filters, Gabor filter banks, and Morphological operators. Next, nonlinear sub-features are extracted from contextual features using convolution filters. Finally, a subset of the reduced feature vector is produced using a fully connected layer which is then fed to a classifier. The accuracy rate of 76% and 94% were obtained from CT scans and X-ray images respectively.

2.2 Deep Learning Methods

Deep learning (DL) methods are based on new structured algorithms to develop methods and intelligent machines requiring less human interaction. DL is a part of the machine learning domain having numerous applications in the medical profession such as Myocardial infarction detection [32, 33]. Recently the use of DL methods for COVID-19 pandemic solutions has increased because of their impressive classification performance. Moghaddam and Gholamalinejad [26] proposed a novel deep learning method for COVID-19 detection. Their model is the combination of Squeeze Excitation Block and Pooling layer. To increase the COVID-19 diagnosis performance, they use Mish Function and Batch Normalization to optimize the convergence time. Experiments were performed on two public hospital datasets and the recognition accuracy rate of 99% was reported. In 2021, Panthakkan et al. [27] provided a highly efficient and novel method named COVID-DeepNet for rapid and accurate detection of COVID-19 which was reported to work as a multi-class classification of X-ray images into normal (healthy), non-COVID Pneumonia, and COVID-19. An accuracy rate of 99.67% was observed for the dataset size of 7500 images. Kassania et al. [28] have performed a comparison of popular deep learning methods like NASNET, VGGNet, InceptionResNetV2, InceptionV3, ResNet, Xception, DenseNet, and MobileNet for automatic classification of COVID-19. The deep learning-based extracted features are then passed to multiple classifiers to classify the patient as either a case of non-COVID or COVID-19. They reported the best performance of 99% accuracy rate by using the DenseNet with bagging tree classifier. Serte and Demire [29] designed artificial intelligence (AI) based method to classify COVID-19 and Non-COVID-19 cases. They used ResNet-50 which is a deep learning model to predict the positive COVID-19 cases from 3D CT scan images. After that, image-level predictions are fused with the AI method to detect COVID-19 from 3D CT images.

Rahimzadeh et al. [34] introduced a large COVID-19 infection patient dataset containing 15,589 images of 95 patients with COVID-19 infection and 48,260 CT scan images of 282 normal persons. First, they discarded some of the lung images with low visibility using an image processing algorithm. Secondly, they strengthened the ResNet50V2 model using a new feature pyramid network that can investigate different resolution images without loss of small objects data. The accuracy rate of 98.49% is achieved during the single image classification stage. Maharjan et al. [35] used six CNN architecture, Inception V3, NasNet-Mobile, MobileNet, DenseNet201, DenseNet121 and VGG16. They studied six models to train the generic images and the seventh model (DenseNet121) was trained on CXR images. Furthermore, fully connected layers were introduced in replacement of output layers for binary classification of COVID-19.

The approach presented in [36] employs a Weakly-supervised deep active learning model named COVID-AL for COVI-19 detection from CT scan images. In this method, the authors used a 2D U-Net

for lung region segmentation and a new active learning method is used for COVID-19 diagnosis. This approach not only considers predicted loss but also samples diversity. They have reported the classification accuracy rate of 95% overusing the complete dataset with only 30% of labeled data. To detect the varying degrees of COVID-19 from chest CT scans the author in [37] proposed a model named ReCOV-101. The interpolation and segmentation operation are employed for detection accuracy rate improvement. Their model consists of a residual network with skip connection capability which gives the model an edge to go deeper. Similarly, Kedia et al. [38] developed an Ensemble Deep CNN model that can extract the important characteristics from X-ray images to detect the COVID-19. The average classification rate of 98.28% is obtained for three-class classification that is Normal, Pneumonia, and COVID-19. Nigam et al. [39] have presented a deep learning architecture like EfficientNet, NASNet, Xception, DenseNet121, and VGG16 to develop a COVID-19 detection system. The classes used in this method are normal patients, positive patients, and other classes. The other class is related to illnesses, influenza, and pneumonia. The average accuracy rate for EfficientNet, NASNet, Xception, DenseNet121 and VGG16 are 93.48%, 85.03%, 88.03&, 89.96% and 79.01% respectively. In [40], the authors considered four pre-trained deep learning models: WideResNet 50 2, DenseNet 169, ResNet 101 and VGG 19 for automatic detection of COVID-19. They varied the fully connected layers in number to obtain the potential candidates for base classifiers. The three best models were selected based on their performance for the heterogeneous stacked ensemble. Goyal and Singh [41] used machine learning and deep learning technique for the early detection of COVID-19. They first used a median filter followed by the histogram equalization to enhance the image quality. After that, a modified region growing technique is utilized for accurate ROI extraction. Features such as intensity, texture, shape and visual features are then extracted from the ROI region. In [42], the authors proposed a novel deep transfer learning model for the accurate detection of COVID-19. Various transfer learning models such as XceptionNet, GoogLeNet, and EfficientNet are ensembled to categorize the patient as healthy, tuberculosis, pneumonia, and COVID-19. The model proposed in this work enhances the classifier ability for binary and multiclass COVID-19 datasets. Similarly, in [43], a transfer learning method is implemented for the classification of COVID-19 from X-ray images. EfficientNetB0, ResNet50, and VGG16 are used in this work as feature extractors. In another study [44], three deep learning models namely VGG16, InceptionV3, and ResNet50 are fine-tuned on the dataset for accurate classification of COVID-19. To increase the number of sample images for experiment, they also performed data augmentation techniques. Table 1 show the summary of the existing techniques.

Considering the significance of COVID detection, the main contribution of this work is highlighted as follow:

- A novel hybrid framework has been developed for automated COVID disease classification.
- Two computationally efficient diverse deep learning models are used to capture variations among significant features.
- Significant hand-crafted features, carrying micro-variation within an image and preserving local information, are extracted.
- Deep learning along with handcrafted features are fused and Entropy-based feature selection has been applied which further reduces feature set size.
- A highly robust and efficient framework has better accuracy using a smaller number of features in comparison to conventional state-of-the-art techniques.
- The rest of the paper is organized as follows: Next section presents the details of the material and methods. In Section 4, the experiments and the result of the proposed method is presented. The conclusion of the work is described in Section 5.

3 Materials and Methods

The overall working framework of the proposed method is depicted in Fig. 1. The Fig. 1 shows that the proposed method begins with the image contrast enhancement. For this purpose, a CLAHE method is employed. Then a feature extraction process takes place in the next step. The hand-crafted features are extracted from X-ray images using WLD and only excitation component features are used. CNN-based inception Resnet101 and DenseNet201 model is employed for deep learning features. These features are fused using concatenation. As a result, a large

Table 1 Comparative analysis of ulcer detection methods

Ref.	Technique	Performance	Important points
Maheshwari et al. [22]	Local binary pattern (LBP)	Average accuracy rate: 97.97%	➢ Texture features are extracted from the images ➢ The proposed method is highly accurate, fast, and contact-free.
Tuncer et al. [23]	Residual Exemplar Local Binary Pattern (ResExLBP)	Average accuracy rate 100% with 10-fold cross-validation	➢ This method is highly accurate, cognitive, and lightweight.
Mostafiz et al. [24]	Deep CNN + DWT features	Average accuracy rate: 98.5%	➢ Mutual information-based feature selection ➢ They reported good performance for unbalanced and overlapping data using ensemble classifier
Pustokhina et al. [25]	DWT + Rough neural network	Average accuracy rate: 80.26%	➢ The pre-processing step was performed to enhance the image quality ➢ Features reduction is carried out to reduce the time complexity
JavadiMoghaddam et al. [26]	DNN	Average accuracy rate: 99.03%	➢ They decreased trend entropy in loss and accuracy
Panthakkan et al. [27]	COVID-DeepNet	Average accuracy rate: 99.67%	➢ This method shows better performance for multi class problems ➢ The proposed model is also efficient as compared to other methods
Jangam et al. [40]	Transfer learning	Average accuracy rate: 84.73%	➢ The proposed model is tested on five different datasets ➢ The DenseNet 169 and VGG 19 is stacked ensemble in this model
Goyal and Singh et al. [41]	F-RNN-LSTM	Average accuracy rate: 95%	➢ Image quality is enhanced followed by ROI based feature extraction ➢ The good accuracy rate is obtained with low computational efforts

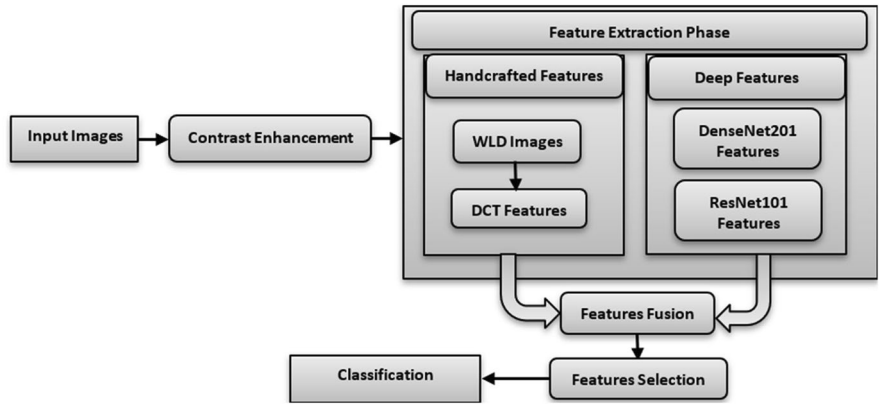

Fig. 1 Schematic diagram of the Proposed method

feature vector is formed. An entropy-based feature reduction is used to select the most significant features. Classification is performed as the last step. The details of the proposed method have been provided in the subsections.

3.1 Pre-processing

It is well known that the quality of the medical image is low during image retrieval processes, storage, transmission, and data acquisition. This leads to lung regions suppressions during the detection

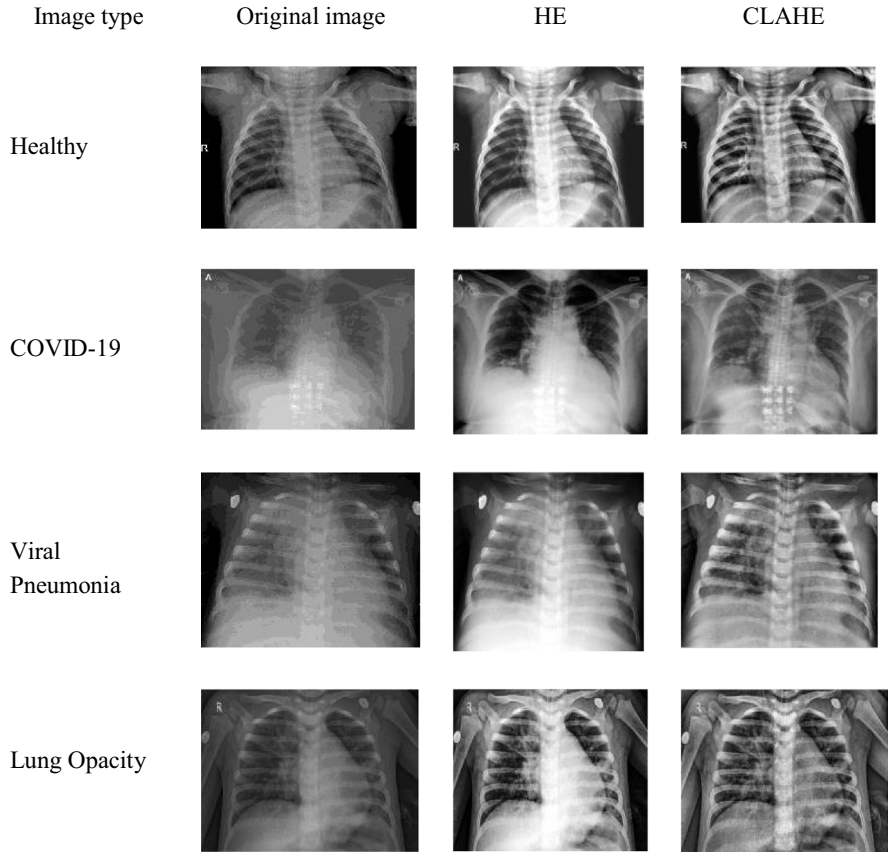

Fig. 2 Image contrast enhancement using HE and CLAHE

process. In literature, most of the research directly employs deep learning models without image contrast enhancement [41]. This, however, greatly reduces performance because it is hard to extract meaningful information from a region of interest due to low intensity. Consequently, there is a compelling need for contrast enhancement methods such as histogram equalization and its variants. Moreover, many studies proved in the literature that the pre-contrast enhancement significantly improves classification accuracy [45]. To enhance the image contrast and reduce the effect of noise, we employed contrast-limited adaptive histogram equalization (CLAHE) in the first step of the proposed method. In the CLAHE method, the most frequent intensity values are effectively spread throughout the images. The traditional histogram equalization method considers the global contrast of an image which leads to over-enhancement and results in an increase in noise as well [46]. CLAHE tends to limit the over-amplified noise that is mostly introduced by AHE [47]. The histogram slope act as a controlling factor for noise amplification.

The image is divided into smaller blocks called "tiles" in CLAHE and then a general histogram equalization mechanism is used to spread the intensity values to that region. However, there is a probability that the noise in the small region gets amplified. To prevent this, *clipLimit* is used in CLAHE. Therefore, if the histogram bins exceed the specified range, then *clipLimit* is used to control it. During the experiments, we have tested different *clipLimit* values for medical images and picked the best performance value.

Figure 2 demonstrates the impact of CLAHE and HE on the low contrast images. It is observed from the experiment that CLAHE performance is better than the HE method in such circumstances. However, the HE method not only increases the image contrast but also boosts the noise to some extent.

3.2 Weber Local Descriptor (WLD)

WLD has proved to be a powerful local texture descriptor. Chen et al. [48] originally proposed WLD

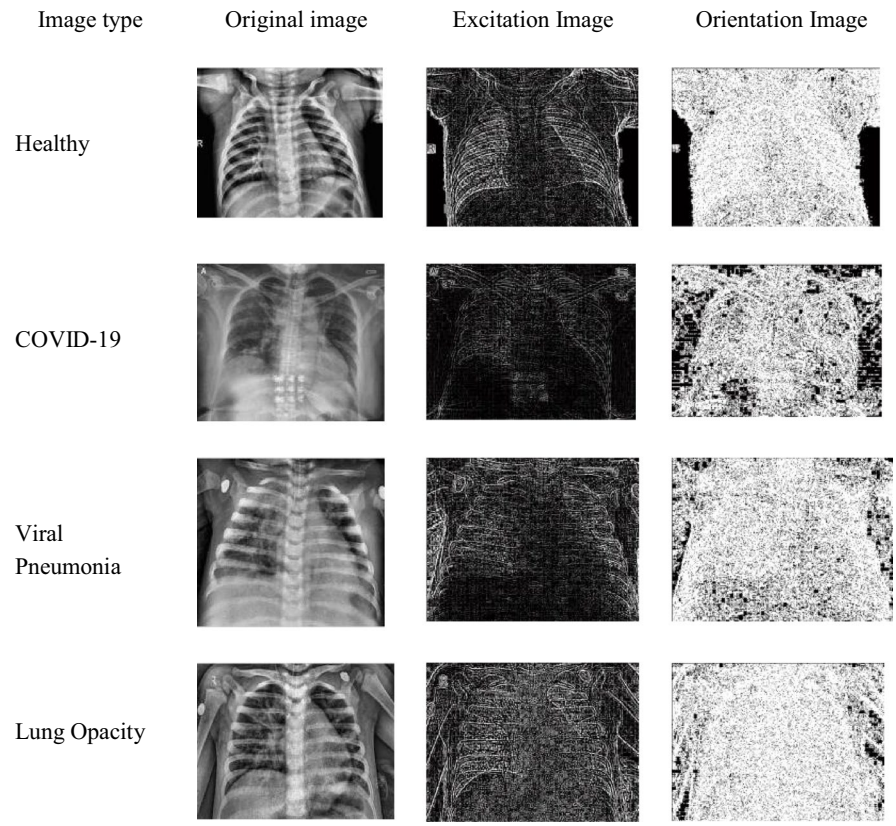

Fig. 3 The excitation and orientation image of WLD

which is based on Weber's law. The law states that there is a constant relationship between background intensity and incremental threshold. WLD mainly consists of (a) differential excitation "ξ" and (b) orientation "Θ". For a given pixel, the excitation component can be computed as the center pixel relative intensity differences ratio against its neighbor's pixel. The changes of the center pixel are represented by the intensity differences between a center pixel and its neighbors. WLD has the ability to resist illumination change and noise.

(a) Differential Excitation: Differential excitation is defined as the ratio of central pixel value to its eight neighboring pixels. It captures the minute variation of a pixel value from its neighborhood and is referred to be as micro features [48]:

$$\xi(x_c) = \arctan\left[\sum_{i=0}^{p-1}\left(\frac{x_i - x_c}{x_c}\right)\right] \quad (1)$$

Here in Eq. (1), n denotes the number of neighboring pixels depending upon the radius taken and i represents the total number of neighbors ranging from $0,1,\ldots\ldots n-1$. Results are further smoothed by applying *arctan* function. In addition to carry global information this excitation component specially focusses on preserving local information. Positive and negative values of differential excitation exhibit the darker and lighter with respect to the neighbor pixel respectively.

(b) Orientation: For a given pixel, the ratio of change between horizontal and vertical direction is represented by the orientation component which can be obtained using the Sobel operator and can be computed as follow [48]:

$$\Theta(x_c) = \arctan\left(\frac{x_7 - x_3}{x_5 - x_1}\right) \quad (2)$$

Orientation component is computed using x_1, x_3, x_5 and x_7.

Figure 3 shows that the excitation image of WLD contains micro-variation within an image which is more useful for classification as compared to orientation image features. As shown in Fig. 3, the local significant patterns are visible in the excitation image. The orientation component is generally used to describe the local direction information in the image. In this work, we only extract the DCT features from the excitation component of WLD.

3.3 Feature Selection using Discrete Cosine Transform (DCT)

DCT is a lossy compression algorithm mainly used for image separation into difference frequencies parts [49]. DCT transforms the spatial domain image into the frequency domain. It represents the data in the sum of the cosine function at different frequencies. In DCT, the less important frequencies are discarded and the most important frequencies are preserved [50]. DCT carries a good energy concentration feature which gives the advantage to process the vibration signal. The noise mainly resists the high-frequency coefficient after we apply the DCT to an input image thus can be easily removed by filtering the high-frequency coefficients. To reduce the processing time and the number of pixels to be processed, we first divide the WLD excitation image into 8×8 blocks. The DCT is employed in each block in a zigzag pattern to get the DCT coefficients in increasing order of frequencies. The DCT of an input image f can be computed as follow:

$$F(u,v) = \alpha_u.\alpha_v.\sum_{x=0}^{N-1}\sum_{y=0}^{M-1}\left[cos\left(\frac{\pi u}{2N}(2x+1)\right)\right] .cos\left(\frac{\pi v}{2M}(2y+1)\right).f(x,y) \quad (3)$$

Where, $f(x,y)$ is a pixel intensity of an input image with x row and y column, the value of $u = 0,1,,\ldots.N-1$ and$v = 0,1,\ldots\ldots,M-1$

$$\alpha_u = \begin{cases}\sqrt{\frac{1}{N}} for u = 0\\ \sqrt{\frac{2}{N}} for u \geq 0\end{cases} \quad \alpha_v = \begin{cases}\sqrt{\frac{1}{N}} for v = 0\\ \sqrt{\frac{2}{N}} for v \geq 0\end{cases}$$

Discrete Cosine Transform (DCT) has the ability of relocating the features having high variance along the top left corner [51] in a zigzag manner. The values near the top left corner have the high energy thus having higher variance. So, it can be best utilized to discriminate among different classes.

3.4 Deep Learning

Deep learning methods have emerged as a useful method for COVID-19 detection. Deep learning generally consists of three layers [52]. The first and the most basic layer of deep learning is the convolution layer. In this layer, different filters are used on the patterns, and then feature maps are created. These filters are capable to generate a wide variety of features. The second layer is the pooling layer which aims is to reduce the size of the feature map and network parameters. The final layer is named a fully connected layer, in which the feature maps are transformed into one-dimension vectors. Our proposed method consists of two deep learning frameworks: ResNet101 and DensNet201. The working of ResNet101 [53] is based on Residual links. This straightforwardly streams the angles over to hinder the slopes. There is a total of 101 convolution layers used in ResNet101 altogether.

3.4.1 ResNet101

Residual Network (ResNet) has shown high applicability in the field of computer vision [54, 55]. This network is capable of training really deep networks i.e. up to 1000 layers [56]. ResNet 101 allows the information flow between layers without fading it based on the correlation principle between identical connections [57]. It is a fast CNN model and uses comparatively a smaller number of parameters. The vanishing gradient problem is better handled in this CNN model and hence improves accuracy with fast convergence. In this network model shortcut, connections are taken into account instead of the convolutional layers block approach [53]. The newly adopted approach of shortcut connections is applied when input and output are dimensionally equal. If the dimension differs, we can use two approaches first one is that identity mapping will go with the shortcut connections by padding zeros for the dimensional increment, in this way there would be no increment in parameters. The second approach is to match the dimensions of both input and output by using a projection shortcut it is done with the help of 1×1 convolutional filters. The two common problems faced during the implementation of ResNet-101 are the increase in complexity of the proposed architecture and the second problem is the dependence of ResNet on the implementation of Batch Normalization layers.

One of the equations acting as a building block in this model is given below:

$$Z = F\left(Y, \left\{U_i\right\}\right) + Y \tag{4}$$

Y and Z are the input and output vectors where $F\left(Y, \left\{U_i\right\}\right)$ is the mapping function to be learned whereas $F + Y$ are performed by the shortcut connections.

He et al. [53] used this pre-trained model for image recognition. This model consists of input layer, output layer, softmax, fully connected (FC), average pooling (AP), max polling (MP), 33 additional layers, 104 batch normalization layers, 100 ReLU layers and 104 convolutional layers. This model used the input image size of $224 \times 224 \times 3$. In max-polling operation this model utilizes the padding (0,1,0 and 1), stride (2,2) and pool size (3,3). In average pooling operation the pool and stride size (7,7) are used with zero padding.

The network is trained on the COVID-19 dataset and trained features are extracted. We have selected 2048 features from layer 'pool5' and 1000 features extracted from 'fclayer'.

3.4.2 DenseNet201

DenseNet-201 is a convolutional neural network containing 201 deep layer with modification of the connected between layers [55]. Unlike traditional nets, one layer is connected to all other layers in DenseNet. The multiple densely connected "dense blocks" are used in this architecture which includes activation layers, max pooling, and convolution layer. This architecture was trained for 1000 object classes originally. The concept of skipping layers is also introduced recently in DenseNet201. Total 11 convolution layers followed by 22 average polling layers are used as a transition layer between two contiguous dense blocks. Moreover, the feature map sizes are uniform within the dense block

Table 2 The total number of images before and after the data augmentation step

Class	No. of images before data augmentation step	No. of images after data augmentation step
COVID	3616	14,464
Lung Opacity	6012	12,024
Normal	10,192	10,192
Viral	1345	10,760

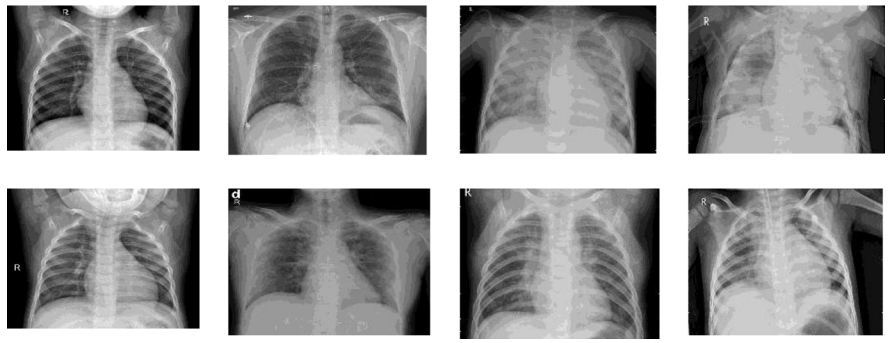

(a) (b) (c) (d)

Fig. 4 Sample images of database. **a** Healthy. **b** COVID-19. **c** Viral pneumonia. **d** Lung opacity

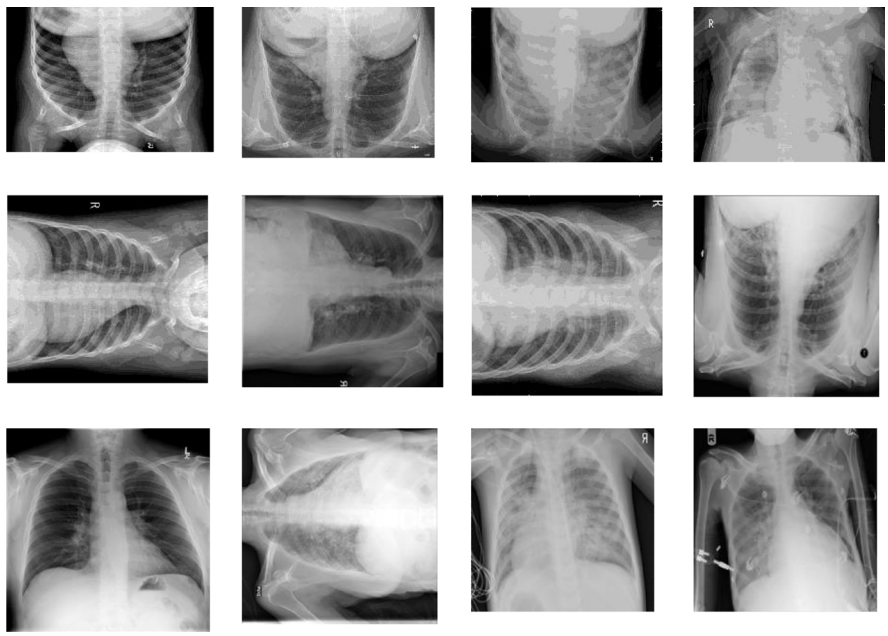

(a) (b) (c) (d)

Fig. 5 Augmented Sample images of database. **a** Healthy. **b** COVID-19. **c** Viral pneumonia. **d** Lung opacity

which allow to readily concatenated. At the last dense block conclusion, global average pooling is performed and then softmax classifier is added. In this model the features from all levels of complexity are incorporated by the classifier which make the network to provide more accurate decisions. The input image size of this model is 224×224.

4 Experimentation and Results

To evaluate the performance of the proposed technique using covid19-radiography-database is used for classification. The dataset consists of 11,993 images of four different types namely COVID (3616), Lung Opacity (6012), Normal (1020), and Viral pneumonia (1345). There is a varying number of images in each class and the dataset is imbalanced. Data augmentation is applied to handle the issue of imbalance and to overcome overfitting. Flip and rotate operations are performed to enhance the dataset. The maximum class was set as a threshold and other classes were augmented as per the selected threshold value. The maximum class is Opacity containing 6012, thus the other classes were COVID (3616), Normal (1020), and Viral pneumonia (1345). The threshold is calculated using Eq. 5;

$$T = \max\left(C_i\right) \tag{5}$$

Where C denotes the classes and $i = 1, \ldots, 4$. T is a threshold value containing the maximum number of images in a single class. The number of images in other classes is compared with T and the augmentation ratio is calculated which was used to enhance the dataset. Table 2. Illustrate the total number of images before and after augmentation.

A sample of images from an original dataset with different classes is shown in Fig. 4 and augmented images of the database are shown in Fig. 5.

We used Matlab 2020a to conduct our experiments using core i-5, 7th generation with 16GB RAM, and NIVIDIA RTX-1080 2GB. We adopted a ratio of 70:15:15 for training testing and validation, Maximum epochs were set at 300 with 30 iterations per epoch. Fivefold cross-validation was used to reduce the biases.

4.1 Performance Evaluation Metrics

Performance of the system is evaluated using well known performance metrics like Precision, Recall and Accuracy. All these above-mentioned metrics are based on four measure namely True Positive (TP): If true and predicted true also by the classifier, False Positive (FP): actually, negative but predicted as positive, True Negative (TN): Sample is negative and also predicted negative and False Negative (FN): sample is positive actually but predicted negative by the predictor;

$$Accuracy = \frac{TP + TN}{TP + TN + FP + FN} \tag{6}$$

$$Precision = \frac{TP}{TP + FP} \tag{7}$$

$$Recall = \frac{TP}{TP + FN} \tag{8}$$

To analyze the model performance, the confusion matrix is one of the essential tools, which represent results in form of predicted vs. true class labels. The confusion matrix is capable to shows the relation among various classes by calculating the performance of each class. In the confusion matrix, the correct classification of each category is represented as a diagonal element.

4.2 Analysis of WLD Results

Figure 6 shows the classification accuracy rate for three features sets (FS) that is FS-128, FS-256, and FS-512. We have large feature dimensions and training and testing such data using quadratic optimization is inefficient

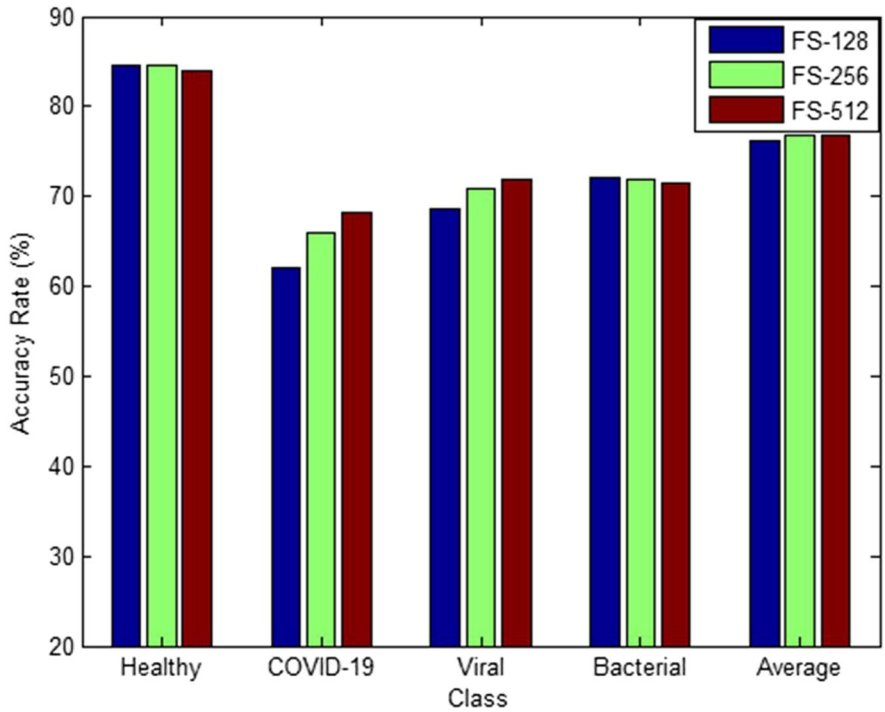

Fig. 6 Classification accuracy rate on different feature sets using WLD

Table 3 Confusion matrix showing the WLD features detected and actual class results using 128 features set

	Detected class				
Actual class		COVID-19	Lung opacity	Healthy	Viral pneumonia
	COVID-19	**61.97**	9.92	26.71	1.38
	Lung opacity	4.87	**71.97**	22.7	0.44
	Healthy	5.18	9.32	**84.59**	0.9
	Viral pneumonia	17.1	1.93	12.26	**68.69**

The bold value indicate the correctly detected class

Table 4 Confusion matrix showing the WLD features detected and actual class results using 256 Features set

	Detected class				
Actual class		COVID-19	Lung opacity	Healthy	Viral pneumonia
	COVID-19	**65.9**	9.5	22	1.7
	Lung opacity	4.85	**71.78**	22.95	0.39
	Healthy	5.27	9.2	**84.52**	0.99
	Viral pneumonia	15.53	1.48	12.11	**70.85**

The bold value indicate the correctly detected class

Table 5 Confusion matrix showing the WLD features detected and actual class results using 512 Features set

	Detected class				
Actual class		COVID-19	Lung opacity	Healthy	Viral pneumonia
	COVID-19	**68.16**	8.96	21.04	1.82
	Lung opacity	5.14	**71.35**	22.88	0.61
	Healthy	5.59	9.36	**83.89**	1.14
	Viral pneumonia	15.61	1.85	10.78	**71.74**

The bold value indicate the correctly detected class

Table 6 Classifier's accuracy using ResNet101

Classifier	Features		Accuracy	Precision	Recall	Training Time (s)	Prediction Time (s)
	1000	2048					
Cubic-SVM	✓		93.3	92.4	91.9	875	0.34
		✓	93.4	92.5	92.7	923	0.28
Weighted KNN	✓		85.3	87.7	87.0	1027	0.92
		✓	87.5	86.9	86.3	1055	0.87
Gaussian Naïve Bayes	✓		81.9	79.3	80.1	978	0.68
		✓	81.1	81.0	80.5	1089	0.62
Fine Tree	✓		76.4	74.8	75.4	897	0.69
		✓	77.8	78.2	77.3	913	0.64

and costly. Therefore, SMO [58] is selected which works best on data with large dimensions [59]. The SMO and SVM both use quadratic optimization problems (QP), however, the SMO does little manipulation to reduce the training time. In SMO, the data is divided into small chunks and then optimization takes place.

SMO not only reduce the training time as compared to other classifier but also improve the classification accuracy rate. The average accuracy rate obtained for FS-128, FS-256, and FS-512 is 76.1%, 76.9%, and 76.90% respectively. The increased inaccuracy rate with a small margin has been observed with an increase in feature dimension,

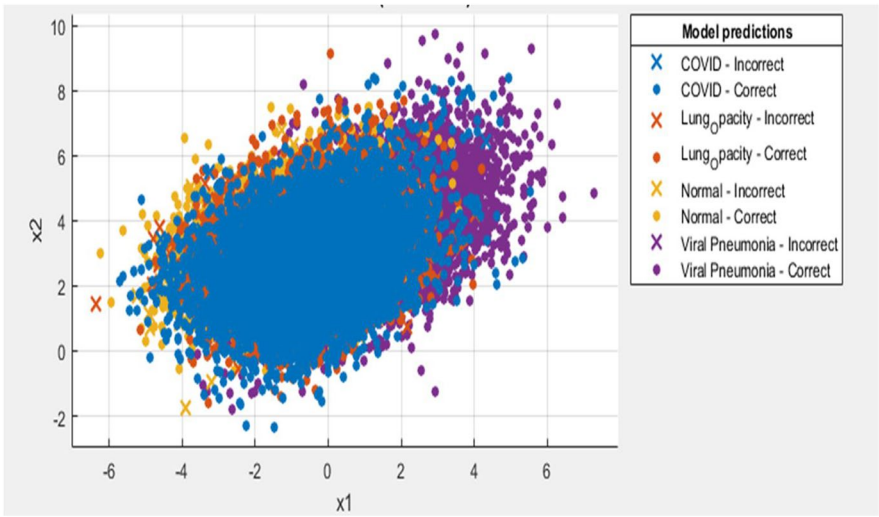

Fig. 7 Scatter plot of ResNet results with 1000 features

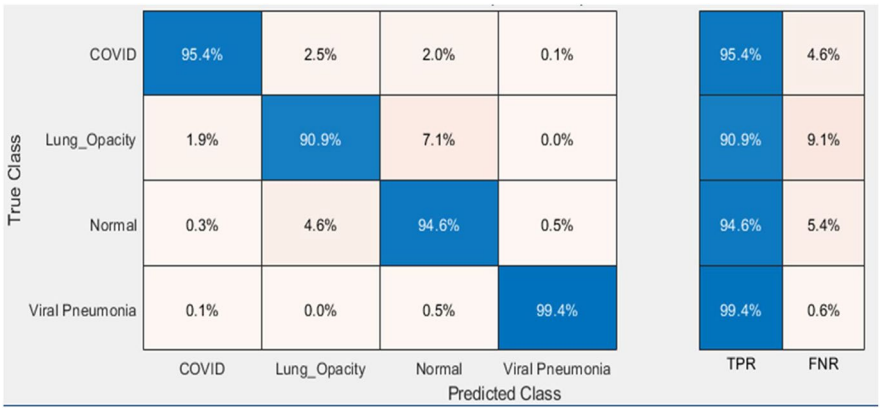

Fig. 8 Confusion matrix of ResNet results with 1000 features

therefore, the small feature set (FS-128) is further utilized for fusion with the deep learning features.

Tables 3, 4, and 5 shows the confusion matrix of different feature set using WLD. From the confusion matrix, the COVID-19 samples are mostly miss-classified with healthy samples. The accuracy rate of the COVID-19 sample is less as compared to Healthy, Lung Opacity, and Viral Pneumonia.

4.3 Analysis of ResNet101 Results

This experiment is performed using features extracted from the fully connected (FC1000) layer which extracted 1000 features per image, while the pool5 layer extracts 2048 features using a pre-trained model ResNet101. The results of this experiment with different classifier accuracy rate comparisons are illustrated in Table 6. The number of extracted features using ResNet101 are 1000 and 2048. It has been observed from the results that cubic-SVM outperform other classifiers by obtaining the accuracy rate of 93.3% and 93.4% for 1000 and 2048 number of features respectively. The result of ResNet101 is also presented in the form of a scatter plot as shown in Fig. 7. The scatter plot shows how well different classes of COVID-19 are distributed. It can be observed from the scatter plot that very few features of COVID-19 classes are misclassified. Moreover, the results of the ResNet101 are also presented in the form of a confusion matrix as shown in Fig. 8. The result shows that the COVID-19 class features are mostly misclassified with Lung Opacity and normal class images. The accuracy rate of COVID-19 classes,

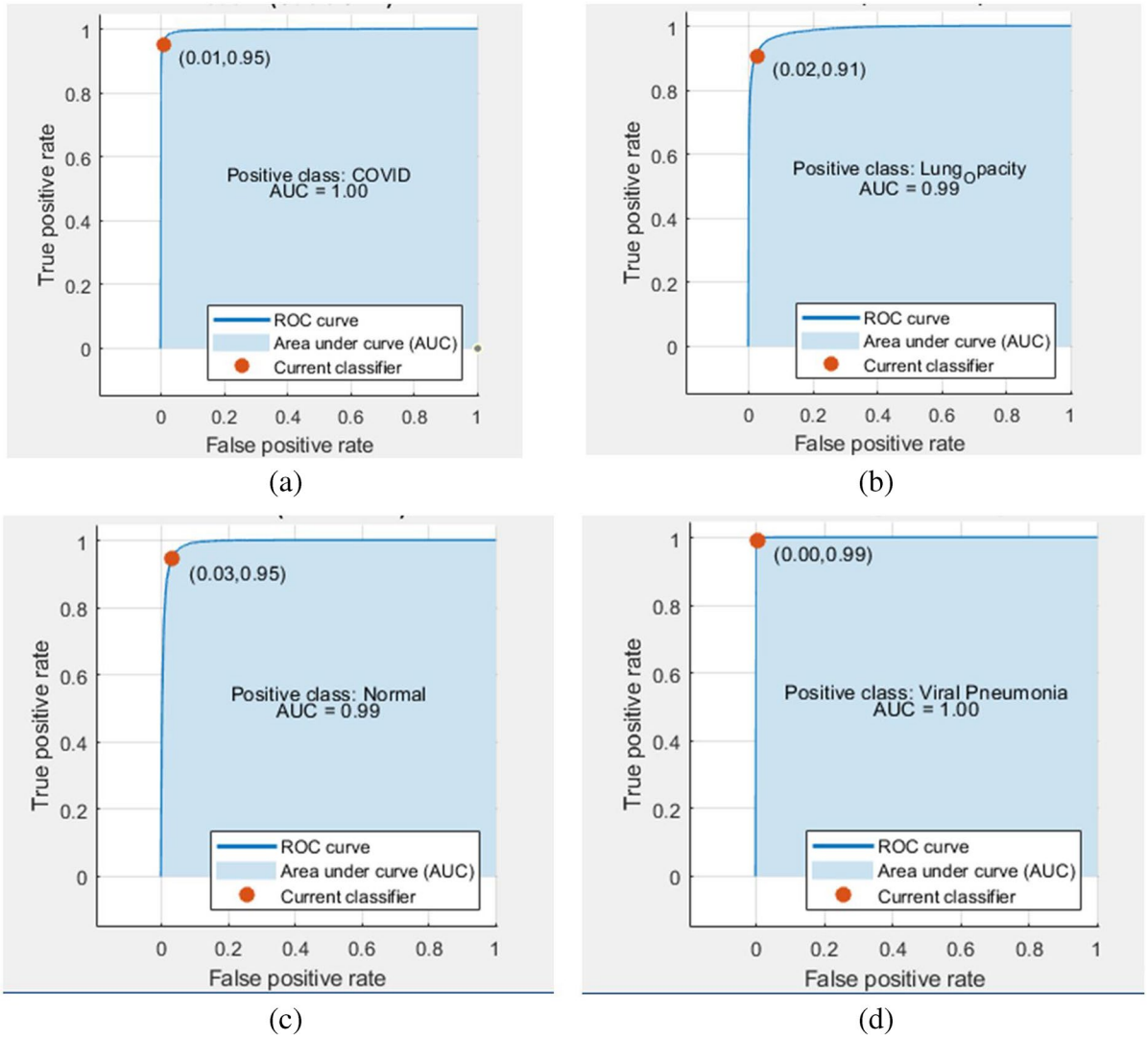

Fig. 9 Representation of ResNet results with 1000 features in terms of ROC plot for different classes. **a** ROC curve for COVID-19 class. **b** ROC curve for Lung Opacity class. **c** ROC curve for Normal class. **d** ROC curve for Viral Pneumonia class

Table 7 Classifier's accuracy using DenseNet201

Classifier	Features		Accuracy	Precision	Recall	Training Time (s)	Prediction Time (s)
	1000	2048					
Cubic-SVM	✓		91.7	91.1	90.9	989	0.30
		✓	92.3	92.7	92.2	1043	0.43
Weighted KNN	✓		87.2	86.3	87.7	1136	0.66
		✓	88.7	87.1	88.4	1267	0.69
Gaussian Naïve Bayes	✓		78.7	78.6	77.9	913	0.67
		✓	81.6	80.9	79.7	1077	0.74
Fine Tree	✓		76.7	76.2	77.3	933	0.92
		✓	78.4	77.8	77.5	991	0.84

Lung Opacity, normal and viral pneumonia is 95.4%, 90.9%, 94.6%, and 99.4% respectively. The results indicate that the Lung Opacity class features accuracy rate is less as compared to all other classes. The images of this class is mostly confused with the health (normal) images. Figure 9 shows the receiver operating characteristic (ROC) curve for the true positive rate and false positive rate of each class. In ROC, the TP rate of the data is plotted against the FP rate with various threshold settings, and the classifier performance is represented by AUC. The higher value of AUC indicates the correctness of the model at distinguishing between non-COVID-19 and COVID-19 cases. The trapezoidal integration is performed to estimate the area under the ROC curve.

4.4 Analysis DensNet201 Results

Table 7 presents classification results after applying DensNet201. For performance measures, the results are compared using cubic-SVM, weighted KNN, Gaussian Naïve Bayes, and fine tree classifiers. In this experiment, the cubic-SVM also showed a higher accuracy rate (i.e., 91.7% for 1000 features and 92.3% for 2048 features) as compared to other classifiers. However, the accuracy rate of DensNet201 on cubic-SVM is lower than ResNet101 (see Table 6). The computed accuracy for weighted KNN, Gaussian Naïve Bayes, and fine tree classifier is 88.7%, 81.6%, and 78.4% respectively. Several other performance measures like precision, recall, training, and testing time are also computed to support the DensNet201 performance. The higher achieved value for precision and recall is 92.7% and 92.2%. The results indicate that the prediction time (i.e., 0.30 s) of cubic-SVM is less as compared to other classifiers. The scatter plot, confusion matrix, and Roc curve are also given in Figs. 10, 11, and 12.

4.5 Analysis of ResNet101 + DensNet201 + WLD Combine Results

After the performance comparison of each deep network, we have also combined the features of ResNet101,

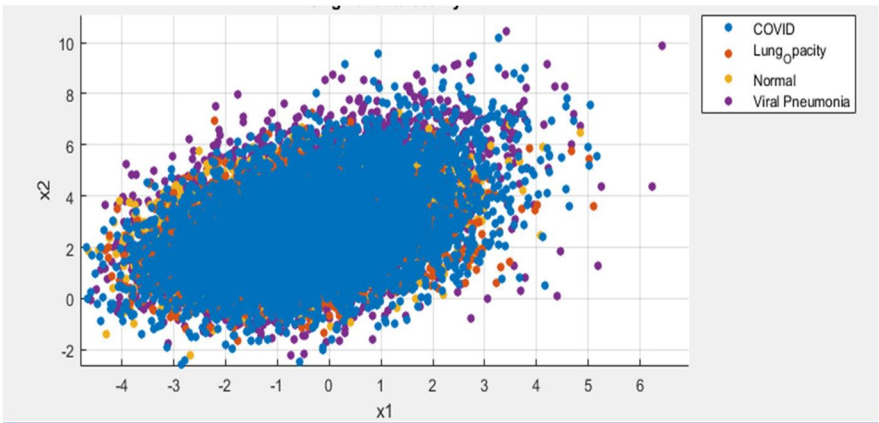

Fig. 10 Scatter plot of DenseNet results with 1000 features

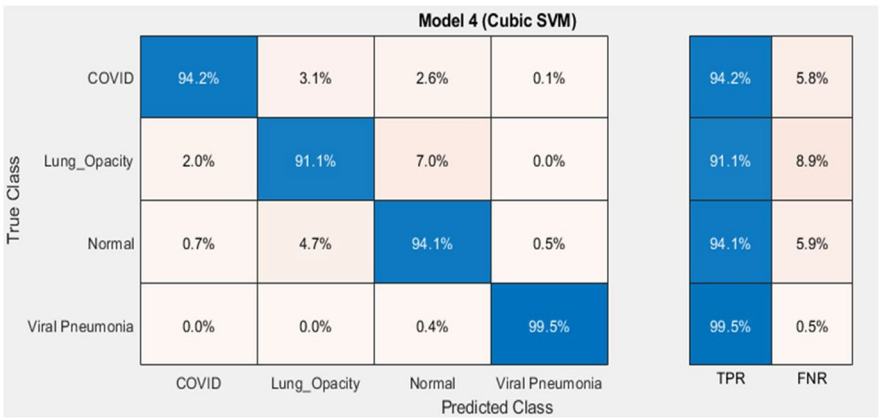

Fig. 11 Confusion matrix of DenseNet results with 1000 features

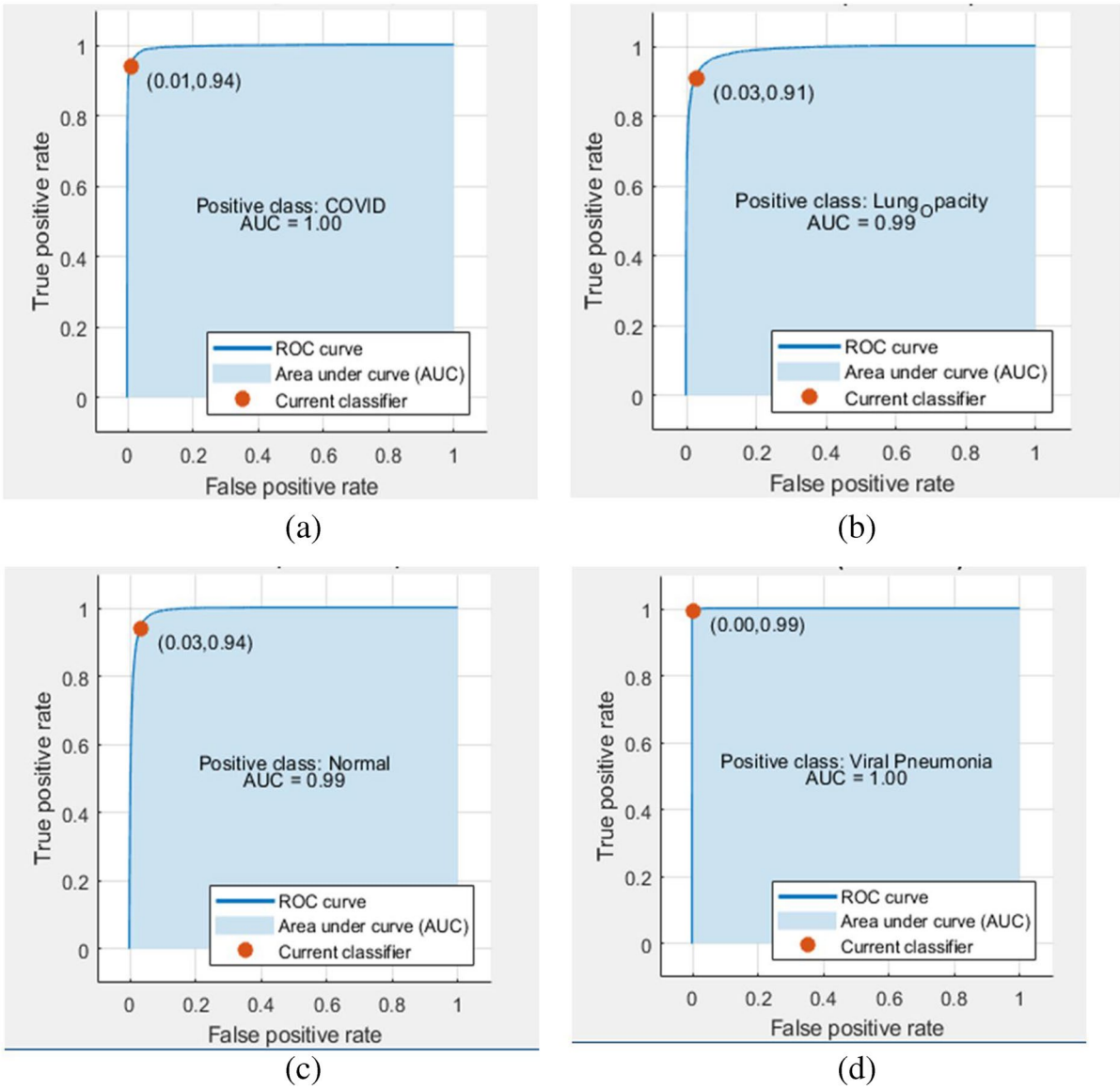

Fig. 12 Representation of DenseNet results with 1000 features in terms of ROC plot for different classes. **a** ROC curve for COVID-19 class. **b** ROC curve for Lung Opacity class. **c** ROC curve for Normal class. **d** ROC curve for Viral Pneumonia class

Table 8 Classifier's accuracy using feature selection over Fused feature vector of ResNet101, DenseNet201 and WLD-DCT

Classifier	Accuracy	Precision	Recall	Training time (s)	Prediction time (s)
Cubic-SVM	99.3	99.7	99.1	387	0.12
Weighted KNN	97.7	96.9	97.2	547	0.33
Gaussian naïve Bayes	98.3	97.4	98.4	464	0.42
Fine tree	98.4	97.2	97.9	412	0.24

Table 9 Proposed method compared with other methods using different databases

Study	Method	Dataset	Accuracy
Ozturk et al. [60]	DarkCovidNet	114 COVID-19 521 No-Findings 490 Pneumonia	2-class (Covid-19 and No-Findings): 98.08% 3-class (Covid-19, No-findings and Pneumonia): 87.02%
Apostolopoulos and Mpesiana [61]	VGG19	224 Covid-19, 714 pneumonia 504 normal	2-class (Covid-19 and others): 96.78% 3-class (Covid-19, pneumonia and normal): 94.72%
Autee et al. [62]	StackNet-DenVIS	168 Covid-19 1596 Non-Covid	2-class (Covid-19 and Non-Covid): 95.07%
Waheed et al. [63]	CNN with synthetic augmentation	72 Covid-19 120 Non-Covid-19	2-class (Covid-19 and Non-Covid): 95.00%
Proposed method	ResNet101 + DenseNet201 + WLD	14,464 Covid-19 10,192 Healthy 10,760 Viral Pneumonia 12,024 Lung Opacity	4-class (Covid-19, health, Virial Pneumonia, Bacterial Pneumonia): 99.3%

DensNet201 and WLD excitation component to acquire more informative combined features. Appropriately combining two or more features' sets can help in decreasing the impact of the inadequate feature of a single CNN model. In this study, a total of 2000 features are obtained using ResNet101 and DensNet201 and 128 features are extracted from WLD images. All these three types of features are combined to generate a feature vector of size (1000 + 1000 + 128 =) 20,128. Entropy-based features are selected from the combined features to reduce the feature vector size up to 1000. This step not only improves the classification accuracy rate but also decreases the computational cost as shown in Table 8. The peak accuracy rate of 99.3% is obtained using cubic-SVM. Similarly, the weighted KNN, Gaussian Naïve Bayes, and fine tree classifier accomplish the accuracy rate of 97.7%, 98.3 and 98.4%.

4.6 Comparison with Existing Methods

The results of the different deep learning models and datasets used in the literature are analyzed in Table 9. In literature, the studies of COVID-19 are generally carried out with two or three classes. Where, healthy and Covid-19 class used as a two-class problem and healthy, pneumonia, Covid-19 class consider as a three-class problem. It will be misleading to directly compare the method results with each other because a different number of images of different classes are used in the studies. We can see from the comparison results that our proposed method achieved the highest accuracy rate of 99.3% despite using four classes.

5 Conclusion and Future Work

The detection of COVID-19 using machine intelligent methods efficiently and reliably is a significant challenge. In this paper, a novel approach is presented for efficient COVID-19 classification using the radiography image dataset. The proposed method relies on features extracted from handcrafted and deep learning features. In the first step, two well-known deep learning models are deployed. Trained features are extracted from both models. Using ResNet101 model 1000 and 2048 features are extracted from fc1000 and pool5 respectively. Similarly, DenseNet201 1000 and 1920 trained features are extracted. WLD features are extracted, and DT-based reduction uses only 128 features. Results of all the individual feature sets are tested. Features are fused using all the combinations and results are compiled. It has been observed that using handcrafted and deep learning features fusion and classification there is improvement in the classification accuracy and time. Significant features are reduced using entropy. The proposed method is tested on 5-fold cross-validation. 99.3% accuracy has been achieved using only 1000 features. The proposed algorithm has proven to be accurate both visually and empirically. The major contribution is improved accuracy using a smaller number of significant features and hence less training and testing time. Data augmentation has played a role in the development of a robust system.

In WLD, only the horizontal and vertical directions are considered while computing differential excitation and orientation components and thus it fails to

fully express the local information of an image. In the future, we plan to further enhance the proposed model by also considering the principal local structure information. We will also investigate the proposed method with additional datasets with multiple classes.

Acknowledgements The authors extend their appreciation to the Deputyship for Research & Innovation, Ministry of Education in Saudi Arabia for funding this research work through the project number 7970.

Declarations

Conflict of Interest The author declares no conflict of interest.

References

1. WHO Lists two COVID-19 tests for emergency use. https://www.who.int/news-room/detail/07-04-2020-who-lists-two-covid-19-tests-for-emergency-use. Accessed 7 Apr 2020
2. Wong, H.Y.F., Lam, H.Y.S., Fong, A.H.T., Leung, S.T., Chin, T.W.Y., Lo, C.S.Y., Lui, M.M.S., Lee, J.C.Y., Chiu, K.W.H., Chung, T.W.H., Lee, E.Y.P.: Frequency and distribution of chest radiographic findings in patients positive for COVID-19. Radiology **296**(2), E72-E78 (2020)
3. Organization, W.H.: Advice on the use of point-of-care immunodiagnostic tests for COVID-19: scientific brief, 8 April 2020. World Health Organization (2020)
4. Abou-Nassar, E.M., Iliyasu, A.M., El-Kafrawy, P.M., Song, O.Y., Bashir, A.K., Abd El-Latif, A.A.: DITrust chain: towards blockchain-based trust models for sustainable healthcare IoT systems. IEEE Access. **8**, 111223–111238 (2020)
5. Pandey, S.K., Janghel, R.R.: Recent deep learning techniques, challenges and its applications for medical healthcare system: a review. Neural Process. Lett. **50**(2), 1907–1935 (2019)
6. Cicceri, G., De Vita, F., Bruneo, D., Merlino, G., Puliafito, A.: A deep learning approach for pressure ulcer prevention using wearable computing. Human-centric Comput. Inform. Sci. **10**(1), 1–21 (2020)
7. Masmoudi, Y., Ramzan, M., Khan, S.A., Habib, M.: Optimal feature extraction and ulcer classification from WCE image data using deep learning. J. Soft Comput. 1–14 (2022). https://doi.org/10.1007/s00500-022-06900-8
8. Jin, B., Che, C., Liu, Z., Zhang, S., Yin, X., Wei, X.: Predicting the risk of heart failure with EHR sequential data modeling. IEEE Access. **6**, 9256–9261 (2018)
9. Zhao, A., Qi, L., Li, J., Dong, J., Yu, H.: LSTM for diagnosis of neurodegenerative diseases using gait data. In: Ninth International Conference on Graphic and Image Processing (ICGIP 2017), p. 106155B (2018)
10. Hu, Y.: Design and implementation of abnormal behavior detection based on deep intelligent analysis algorithms in massive video surveillance. J. Grid Comput. **18**(2), 227–237 (2020)
11. Zheng, H., Liu, J., Ren, X.: Dim target detection method based on deep learning in complex traffic environment. J. Grid Comput. **20**(1), 1–12 (2022)
12. Liu, D., Chen, L., Wang, Z., Diao, G.: Speech expression multimodal emotion recognition based on deep belief network. J. Grid Comput. **19**(2), 1–13 (2021)
13. Yildirim, Ã.: A novel wavelet sequence based on deep bidirectional LSTM network model for ECG signal classification. Comput. Biol. Med. **96**, 189–202 (2018)
14. Qian, P., Xu, K., Wang, T., Zheng, Q., Yang, H., Baydoun, A., Zhu, J., Traughber, B., Muzic, R.: Estimating CT from MR abdominal images using novel generative adversarial networks. J. Grid Comput. **18**(2), 211–226 (2020)
15. Saha, A., Zhang, Y.-D., Satapathy, S.C.: Brain tumour segmentation with a muti-pathway ResNet Based UNet. J. Grid Comput. **19**(4), 1–10 (2021)
16. Ramzan, M., Habib, M., Khan, S.A.: Secure and efficient privacy protection system for medical records. Sustain. Comput.: Inform. Syst. **35**, 100717 (2022)
17. 19 Oct 20; https://radiologyassistant.nl/chest/covid-19/covid19-695imaging-findings
18. Hani, C., Trieu, N.H., Saab, I., Dangeard, S., Bennani, S., Chassagnon, G., Revel, M.P.: COVID-19 pneumonia: a review of typical CT findings and differential diagnosis. Diagn. Interv. Imaging. **101**(5), 263–268 (2020)
19. Sedik, A., Iliyasu, A.M., El-Rahiem, A., Abdel Samea, M.E., Abdel-Raheem, A., Hammad, M., Peng, J., El-Samie, A., Fathi, E., Abd El-Latif, A.A.: Deploying machine and deep learning models for efficient data-augmented detection of COVID-19 infections. Viruses **12**(7), 769 (2020)
20. Sedik, A., Hammad, M., Abd El-Samie, F.E., Gupta, B.B., Abd El-Latif, A.A.: Efficient deep learning approach for augmented detection of Coronavirus disease. Neural Comput. Appl. 1–18 (2021). https://doi.org/10.1007/s00521-020-05410-8
21. Panwar, H., Gupta, P., Siddiqui, M.K., Morales-Menendez, R., Singh, V.: Application of deep learning for fast detection of COVID-19 in X-Rays using nCOVnet. Chaos, Solitons Fractals **138**, 109944 (2020)
22. Maheshwari, S., Sharma, R.R., Kumar, M.: LBP-based information assisted intelligent system for COVID-19 identification. Comput. Biol. Med. **134**, 104453 (2021)
23. Tuncer, T., Dogan, S., Ozyurt, F.: An automated residual exemplar local binary pattern and iterative ReliefF based COVID-19 detection method using chest X-ray image. Chemometr. Intell. Lab. Syst. **203**, 104054 (2020)
24. Mostafiz, R., Uddin, M.S., Reza, M.M., Rahman, M.M.: Covid-19 detection in chest X-ray through random forest classifier using a hybridization of deep CNN and DWT optimized features. J. King Saud Univ.-Comput. Inform. Sci. **34**(2), 3226–3235 (2020). https://doi.org/10.1016/j.jksuci.2020.12.010
25. Pustokhina, I.V., Pustokhin, D.A., Shankar, K.: A novel machine learning–based detection and diagnosis model for coronavirus disease (COVID-19) using discrete wavelet transform with rough neural network. Data Science for COVID-19, pp. 597–612. Elsevier, Amsterdam (2021)
26. JavadiMoghaddam, S., Gholamalinejad, H.: A novel deep learning based method for COVID-19 detection from

CT image. Biomed. Signal Process. Control. **70**, 102987 (2021)
27. Panthakkan, A., Anzar, S., Mansoori, S.Al, Al Ahmad, H.: A novel DeepNet model for the efficient detection of COVID-19 for symptomatic patients. Biomed. Signal Process. Control. **68**, 102812 (2021). https://doi.org/10.1016/j.bspc.2021.102812
28. Kassania, S.H., Kassanib, P.H., Wesolowskic, M.J., Schneidera, K.A., Detersa, R.: Automatic detection of coronavirus disease (COVID-19) in X-ray and CT images: a machine learning based approach. Biocybernetics Biomed. Eng. **41**(3), 867–879 (2021)
29. Serte, S., Demirel, H.: Deep learning for diagnosis of COVID-19 using 3D CT scans. Comput. Biol. Med. **132**, 104306 (2021)
30. Verma, A.K., Vamsi, I., Saurabh, P., Sudha, R., Sabareesh, G., Rajkumar, S.: Wavelet and deep learning-based detection of SARS-nCoV from thoracic X-ray images for rapid and efficient testing. Expert Syst. Appl. **185**, 115650 (2021)
31. Imani, M.: Automatic diagnosis of coronavirus (COVID-19) using shape and texture characteristics extracted from X-Ray and CT-Scan images. Biomed. Signal Process. Control. **68**, 102602 (2021)
32. Hammad, M., Alkinani, M.H., Gupta, B., Abd El-Latif, A.A.: Myocardial infarction detection based on deep neural network on imbalanced data. Multimed. Syst. 1–13 (2021). https://doi.org/10.1007/s00530-020-00728-8
33. Alghamdi, A., Hammad, M., Ugail, H., Abdel-Raheem, A., Muhammad, K., Khalifa, H.S., El-Latif, A., Ahmed, A.: Detection of myocardial infarction based on novel deep transfer learning methods for urban healthcare in smart cities, Multimed. Tools Appl. 1–22 (2020)
34. Rahimzadeh, M., Attar, A., Sakhaei, S.M.: A fully automated deep learning-based network for detecting covid-19 from a new and large lung ct scan dataset. Biomed. Signal Process. Control. **68**, 102588 (2021)
35. Maharjan, J., Calvert, J., Pellegrini, E., Green-Saxena, A., Hoffman, J., McCoy, A., Mao, Q., Das, R.: Application of deep learning to identify COVID-19 infection in posteroanterior chest X-rays. Clin. Imaging. **80**, 268–273 (2021)
36. Wu, X., Chen, C., Zhong, M., Wang, J., Shi, J.: COVID-AL: The diagnosis of COVID-19 with deep active learning. Med. Image Anal. **68**, 101913 (2021)
37. Rohila, V.S., Gupta, N., Kaul, A., Sharma, D.K.: Deep learning assisted COVID-19 detection using full CT-scans. Internet Things **14**, 100377 (2021)
38. Kedia, P., Katarya, R.: CoVNet-19: A Deep Learning model for the detection and analysis of COVID-19 patients. Appl. Soft Comput. **104**, 107184 (2021)
39. Nigam, B., Nigam, A., Jain, R., Dodia, S., Arora, N., Annappa, B.: COVID-19: Automatic detection from X-ray images by utilizing deep learning methods. Expert Syst. Appl. **176**, 114883 (2021)
40. Jangam, E., Barreto, A.A.D., Annavarapu, C.S.R.: Automatic detection of COVID-19 from chest CT scan and chest X-Rays images using deep learning, transfer learning and stacking. Appl Intell **52**, 2243–2259 (2022). https://doi.org/10.1007/s10489-021-02393-4
41. Goyal, S., Singh, R.: Detection and classification of lung diseases for pneumonia and Covid-19 using machine and deep learning techniques. J. Ambient Intell. Humaniz. Comput. 1–21 (2021). https://doi.org/10.1007/s12652-021-03464-7
42. Kumar, N., Gupta, M., Gupta, D., Tiwari, S.: Novel deep transfer learning model for COVID-19 patient detection using X-ray chest images. J. Ambient Intell. Humaniz. Comput. 1–10 (2021). https://doi.org/10.1007/s12652-021-03306-6
43. Zebin, T., Rezvy, S.: COVID-19 detection and disease progression visualization: Deep learning on chest X-rays for classification and coarse localization. Appl. Intell. **51**(2), 1010–1021 (2021)
44. Guefrechi, S., Jabra, M.B., Ammar, A., Koubaa, A., Hamam, H.: Deep learning based detection of COVID-19 from chest X-ray images. Multimed. Tools Appl. **80**(21), 31803–31820 (2021)
45. Rahman, S., Sarker, S., Al Miraj, M.A., Nihal, R.A., Haque, A.N., Noman, A.A.: Deep learning–driven automated detection of COVID-19 from radiography images: a comparative analysis. Cogn. Comput. 1–30 (2021). https://doi.org/10.1007/s12559-020-09779-5
46. Pizer, S.M., Amburn, E.P., Austin, J.D., Cromartie, R., Geselowitz, A., Greer, T., ter Haar Romeny, B., Zimmerman, J.B., Zuiderveld, K.: Adaptive histogram equalization and its variations. Comput. Vis. Graphics Image Process. **39**(3), 355–368 (1987)
47. Reza, A.M.: Realization of the contrast limited adaptive histogram equalization (CLAHE) for real-time image enhancement. J. VLSI Signal Process. Syst. Signal Image Video Technol. **38**(1), 35–44 (2004)
48. Chen, J., Shan, S., He, C., Zhao, G., Pietikäinen, M., Chen, X., Gao, W.: WLD: A robust local image descriptor. IEEE Trans. Pattern Anal. Mach. Intell. **32**(9), 1705–1720 (2009)
49. Ahmed, N., Natarajan, T., Rao, K.R.: Discrete cosine transform. IEEE Trans. Comput. **23**, 90–93 (1974)
50. Watson, A.B.: Image compression using the discrete cosine transform. Math. J. **4**(1), 81 (1994)
51. Pennebaker, W.B., Mitchell, J.L.: JPEG: Still image data compression standard. Springer Science & Business Media (1992)
52. Goodfellow, I., Bengio, Y., Courville, A.: Deep learning. MIT Press (2016)
53. He, K., Zhang, X., Ren, S., Sun, J.: Deep residual learning for image recognition. In Proceedings of the IEEE conference on computer vision and pattern recognition, pp. 770–778. (2016)
54. Targ, S., Almeida, D., Lyman, K.; Resnet in resnet: Generalizing residual architectures. arXiv preprint arXiv:1603.08029 (2016)
55. Huang, G., Liu, Z., Maaten, L.V.D., Weinberger, K.Q.: Densely connected convolutional networks. In: Proceedings of the IEEE conference on computer vision and pattern recognition, pp. 2261–2269 (2017)
56. He, F., Liu, T., Tao, D.: Why resnet works? residuals generalize. IEEE Trans. Neural Netw. Learn. Syst. **31**(12), 5349–5362 (2020)
57. Srivastava, R.K., Greff, K., Schmidhuber, J.: Training very deep networks. arXiv preprint arXiv:1507.06228 (2015)

58. Platt, J.: Sequential minimal optimization: A fast algorithm for training support vector machines. Advances in Kernel Method: Support Vector Learning, pp. 185–208 (1998)
59. Joachims, T.: Training linear SVMs in linear time, pp. 217–226
60. Ozturk, T., Talo, M., Yildirim, E.A., Baloglu, U.B., Yildirim, O., Acharya, U.R.: Automated detection of COVID-19 cases using deep neural networks with X-ray images. Comput. Biol. Med. **121**, 103792 (2020)
61. Apostolopoulos, I.D., Mpesiana, T.A.: Covid-19: automatic detection from x-ray images utilizing transfer learning with convolutional neural networks. Phys. Eng. Sci. Med. **43**(2), 635–640 (2020)
62. Autee, P., Bagwe, S., Shah, V.: Srivastava,"StackNet-DenVIS: a multi-layer perceptron stacked ensembling approach for COVID-19 detection using X-ray images. Phys. Eng. Sci. Med. **43**(4), 1399–1414 (2020)
63. Waheed, A., Goyal, M., Gupta, D., Khanna, A., Al-Turjman, F., Pinheiro, P.R.: Covidgan: data augmentation using auxiliary classifier gan for improved covid-19 detection. IEEE Access. **8**, 91916–91923 (2020)